WASP-190b: Tomographic Discovery of a Transiting Hot Jupiter

L. Y. Temple[1], C. Hellier[1], Y. Almleaky[2,3], D. R. Anderson[1], F. Bouchy[4], D. J. A. Brown[5,6], A. Burdanov[7], A. Collier Cameron[8], L. Delrez[9], M. Gillon[7], E. Jehin[7], M. Lendl[4,10], P. F. L. Maxted[1], C. Murray[9], L. D. Nielsen[4], F. Pepe[4], D. Pollacco[5,6], D. Queloz[9], D. Ségransan[4], B. Smalley[1], S. Thompson[9], A. H. M. J. Triaud[11], O. D. Turner[1,4], S. Udry[4], and R. G. West[5]

[1] Astrophysics Group, Keele University, Staffordshire, ST5 5BG, UK; l.y.temple@keele.ac.uk
[2] Space and Astronomy Department, Faculty of Science, King Abdulaziz University, 21589 Jeddah, Saudi Arabia
[3] King Abdullah Centre for Crescent Observations and Astronomy (KACCOA), Makkah Clock, Saudia Arabia
[4] Observatoire astronomique de l'Université de Genève 51ch. des Maillettes, 1290 Sauverny, Switzerland
[5] Department of Physics, University of Warwick, Gibbet Hill Road, Coventry, CV4 7AL, UK
[6] Centre for Exoplanets and Habitability, University of Warwick, Gibbet Hill Road, Coventry CV4 7AL, UK
[7] Space sciences, Technologies and Astrophysics Research (STAR) Institute, Université de Liège, Allée du 6 Août 17, B-4000 Liège, Belgium
[8] SUPA, School of Physics and Astronomy, University of St. Andrews North Haugh, Fife, KY16 9SS, UK
[9] Cavendish Laboratory, J J Thomson Avenue, Cambridge, CB3 0HE, UK
[10] Space Research Institute, Austrian Academy of Sciences, Schmiedlstr. 6, A-8042, Graz, Austria
[11] School of Physics & Astronomy, University of Birmingham, Edgbaston, Birmingham, B15 2TT, UK

Abstract

We report the discovery of WASP-190b, an exoplanet on a 5.37 day orbit around a mildly evolved F6 IV-V star with $V = 11.7$, $T_{eff} = 6400 \pm 100\,\mathrm{K}$, $M_* = 1.35 \pm 0.05\,M_\odot$, and $R_* = 1.6 \pm 0.1\,R_\odot$. The planet has a radius of $R_P = 1.15 \pm 0.09\,R_{Jup}$ and a mass of $M_P = 1.0 \pm 0.1\,M_{Jup}$, making it a mildly inflated hot Jupiter. It is the first hot Jupiter confirmed via Doppler tomography with an orbital period of >5 days. The orbit is also marginally misaligned with respect to the stellar rotation, with $\lambda = 21° \pm 6°$ measured using Doppler tomography.

Key words: planets and satellites: detection – planets and satellites: individual (WASP-190b) – stars: individual (WASP-190)

Supporting material: data behind figure, machine-readable table

1. Introduction

The Rossiter–McLaughlin (RM) effect, a distortion of the line profiles of a star caused by an occulting body blocking part of the stellar face, was first detected for a transiting hot Jupiter by Queloz et al. (2000) in observations of HD 209458, whereby the distortion was detected as a perturbation to radial velocity (RV) measurements. It has since been used extensively to measure the projected angle between the planet's orbit and the stellar rotation axis in many hot-Jupiter systems (e.g., Triaud 2017). The current alignment of a planetary orbit with respect to the stellar rotation is an indicator of the dynamical history of the planet, and can point to the formation mechanisms at play.

One can also plot the line profiles as a function of phase, looking for the Doppler shadow of the planet as it moves across the line profiles. The detection of the Doppler tomographic signal of a candidate exoplanet can rule out transit mimics such as blended eclipsing binaries. This tomographic method was first used in the discovery of a planet for WASP-33b (Collier Cameron et al. 2010b). The tomographic technique is particularly useful for systems with hotter and fast-rotating stars, with fewer and broader spectral lines, which may give only less-accurate RV measurements and thus were previously paid less attention by transit and RV surveys. Thus Doppler tomography has now been used in the discovery of hot Jupiters transiting hot stars, including KELT-20b (Lund et al. 2017), HAT-P-67b (Zhou et al. 2017), WASP-167b/KELT-13b (Temple et al. 2017), MASCARA-1b (Talens et al. 2017), and WASP-189b (Anderson et al. 2018).

Brown et al. (2017) compare tomographic and RM analyses of the same data sets for six WASP systems. They find that the tomographic method consistently gives better constraints on values for the projected stellar rotational velocity $v \sin i_\star$ and the sky-projected obliquity angle λ. Note that the tomographic analysis method uses the line profiles more directly, while an RM analysis in terms of RV measurements needs one to translate the change in the line profiles owing to a planet shadow into a change in the overall RV (e.g., Hirano et al. 2011; Boué et al. 2013).

The number of known exoplanets has grown to the point where population studies can draw significant and meaningful conclusions about their bulk properties and dynamical histories. For example, Schlaufman (2018) uses a sample of 146 systems comprised of a solar-like star and a giant planet, brown dwarf, or low-mass stellar companion, to place a mass-limit boundary between hot Jupiters and brown dwarfs that relies on their formation mechanism. It is not possible, however, to perform the same scale of population studies for hot Jupiters orbiting early-type stars, due to the relative lack of such objects discovered so far (resulting, at least partially, from selection biases in past transit and RV surveys).

Hot Jupiters orbiting hot stars are of interest due to the orbital and physical differences between them and hot Jupiters orbiting later-type stars. They are more likely to be in misaligned orbits (Winn et al. 2010; Triaud 2017), often have stars that rotate more quickly than the planet's orbit (e.g., Crouzet et al. 2017; Temple et al. 2017), and are inflated, with hotter dayside temperatures, due to the increased irradiation from their host star (Hartman et al. 2016; Temple et al. 2018).

Table 1
Observations of WASP-190b

Telescope/Instrument	Date	Notes
WASP-South	2006–2011	30137 pts.
TRAPPIST-South	2014 Nov 26	$I + z$, 7 s exp.
SPECULOOS-Europa	2017 Oct 13	$I + z$, 10 s exp.
CORALIE	2014 Aug–Oct	5 RVs
HARPS	2017 Oct 13	28 spectra taken including a transit
HARPS	2018 Oct	5 RVs

The increased irradiation might also result in planetary magnetic fields that are stronger than those in cooler Jupiters, since the continuous injection of energy into the interior of a gas giant might produce a more efficient planetary dynamo (Yadav & Thorngren 2017).

In this work, we report the discovery and characterization of WASP-190b, a hot Jupiter orbiting a star of $T_{\rm eff} = 6400$ K which can be found in *TESS* Sector 2 as TIC ID:116156517 (Ricker et al. 2015; Stassun et al. 2018). We use both tomographic and RM analyses to determine the geometry of the system, and confirm the existence of the planet via the detection of its Doppler shadow and by measuring its mass using orbital RV measurements.

2. Data and Observations

We observed WASP-190 using the WASP-South telescope (Hellier et al. 2011) at the South African Astronomical Observatory (SAAO) from 2006 to 2011. After the detection of a planet-like transit dip in the WASP light curve we confirmed the transit with a follow-up light curve obtained using the TRAPPIST-South telescope (Jehin et al. 2011), and proceeded to obtain reconnaissance spectroscopy with the Euler/CORALIE spectrograph (Queloz et al. 2001). These were sufficient to rule out a stellar-mass binary, but, with relatively large errors, were consistent with no motion at the level of 250 m s^{-1}, and were inconclusive in finding whether or not the transiting body was a planet.

We thus attempted tomography of a transit, obtaining a series of 28 spectra through transit on the night of 2017 October 13 using the European Southern Observatory (ESO) 3.6 m/HARPS spectrograph (Pepe et al. 2002), accompanied by simultaneous photometry using the SPECULOOS-Europa telescope (Burdanov et al. 2018; Delrez et al. 2018; Gillon 2018). After tomographic detection of a planet-like signal, we obtained five further orbital RVs with HARPS to constrain the planetary mass. Details of the observations carried out are given in Table 1.

The HARPS spectra were cross-correlated over a window of ±350 km s^{-1}, using a mask matching a G2 spectral type, and the standard HARPS Data Reduction Software as described by Baranne et al. (1996) and Pepe et al. (2002). We then analyzed the cross-correlation functions (CCFs) themselves, and computed RV measurements from the CCFs which we list in Table 2 along with the bisector spans (BS).

We used the WASP photometric data to look for any evidence of rotational modulation of the host star, using the methods of Maxted et al. (2011). We find no such variability at periods longer than a day, with a 95% confidence upper limit on the amplitude of 1 mmag.

Table 2
RV Measurements of WASP-190, Taken Using the CORALIE and HARPS Spectrographs for This Work

$\mathrm{BJD_{TDB}}$ −2,450,000	RV (km s^{-1})	$\sigma_{\rm RV}$ (km s^{-1})	BS (km s^{-1})	$\sigma_{\rm BS}$ (km s^{-1})
CORALIE (Out of Transit):				
6871.794771	0.89	0.05	−0.07	0.10
6895.811527	0.94	0.05	−0.16	0.10
6922.731329	0.90	0.03	−0.05	0.06
6952.511870	0.95	0.04	0.15	0.08
7000.625106	0.87	0.04	−0.22	0.08
8392.595422	0.84	0.07	−0.24	0.14
HARPS (Including a Transit):				
8040.529251	0.84	0.02	0.04	0.04
8040.540026	0.82	0.02	−0.04	0.04
8040.550489	0.84	0.02	0.05	0.04
8040.561472	0.86	0.02	−0.02	0.04
8040.572351	0.85	0.02	−0.05	0.04
8040.582918	0.85	0.02	−0.02	0.04
8040.593797	0.87	0.02	−0.00	0.04
8040.604572	0.92	0.02	0.02	0.04
8040.615243	0.89	0.02	−0.07	0.04
8040.626122	0.90	0.02	−0.13	0.04
8040.636897	0.87	0.02	−0.06	0.04
8040.647776	0.84	0.02	−0.01	0.04
8040.658459	0.80	0.02	−0.02	0.04
8040.669130	0.79	0.02	0.04	0.04
8040.680113	0.80	0.02	0.10	0.04
8040.690784	0.80	0.02	0.03	0.04
8040.701350	0.78	0.02	−0.07	0.04
8040.712334	0.76	0.02	−0.03	0.04
8040.723016	0.73	0.02	−0.03	0.04
8040.733791	0.76	0.02	−0.05	0.04
8040.744670	0.73	0.03	−0.05	0.06
8040.755341	0.76	0.03	0.05	0.06
8040.766220	0.77	0.03	0.09	0.06
8040.777100	0.81	0.03	−0.10	0.06
8040.787770	0.83	0.03	−0.02	0.06
8040.798545	0.82	0.03	0.10	0.06
8040.809112	0.85	0.03	−0.06	0.06
8040.820107	0.82	0.03	0.06	0.06
HARPS (Out of Transit):				
8393.843700	0.92	0.01	−0.20	0.02
8396.706300	0.73	0.01	0.10	0.02
8397.590800	0.86	0.04	−0.15	0.08
8398.611000	0.92	0.02	−0.24	0.04
8399.542350	0.85	0.04	−0.13	0.08

(This table is available in machine-readable form.)

3. Stellar Parameters from Spectral Analysis

In order to determine stellar parameters of WASP-190 we co-added the HARPS spectra obtained on the night of 2017 October 13 and performed a spectral analysis. We adopted a microturbulent velocity of $v_{\rm mic} = 1.6$ km s^{-1} from the calibration of Bruntt et al. (2010) and a macroturbulent velocity of $v_{\rm mac} = 6.5$ km s^{-1} from the calibration of Doyle et al. (2014). We used the Hα line to determine an effective temperature of $T_{\rm eff} = 6400 \pm 100$ K, while using the Na D feature to measure $\log g_* = 3.9 \pm 0.1$. We also determined the projected stellar rotational velocity $v \sin i_* = 13.8 \pm 0.7$ km s^{-1}, and the surface metallicity [Fe/H] $= -0.02 \pm 0.05$. These results are also listed in Table 3. Using the MKCLASS program (Gray & Corbally 2014), we then obtained a spectral type of F6 IV–V.

Table 3
All System Parameters Obtained in the Combined Analyses for WASP-190b

1SWASP J003050.23–403424.3
2MASS 00305023–4034243
TIC ID:116156517
Gaia DR2 4994237247949280000
R.A. = $00^h30^m50\overset{s}{.}233$, Decl. = $-40°34'24\overset{''}{.}36$ (J2000)
$V = 11.7 \pm 0.1$ (TYCHO2)
Gaia DR2 Proper Motions:
(R.A.) 38.23 ± 0.03 (decl.) -9.14 ± 0.04 mas yr^{-1}
Gaia DR2 Parallax: 1.82 ± 0.03 mas
Rotational Modulations: <1 mmag (95%)

Stellar Parameters from Spectral Analysis:

Parameter (Unit)	Value
Spectral type	F6 IV–V
$T_{\rm eff}$ (K)	6400 ± 100
$\log g_*$	3.9 ± 0.1
[Fe/H]	-0.02 ± 0.05
$v \sin i_*$ (km s^{-1})	13.8 ± 0.7
$v_{\rm mic}$ (km s^{-1})	1.6 (assumed)
$v_{\rm mac}$ (km s^{-1})	6.5 (assumed)

Parameters from Photometric and RV Analysis:

Parameter (Unit)	DT Value (adopted):
P (day)	5.367753 ± 0.000004
$T_{\rm c}$(BJD$_{\rm TDB}$)	2457799.1256 ± 0.0007
T_{14} (day)	0.186 ± 0.002
$T_{12} = T_{34}$ (day)	0.017 ± 0.002
$R_{\rm P}^2/R_*^2$	0.0062 ± 0.0002
b	0.45 ± 0.09
i (°)	87.1 ± 0.7
a (au)	0.0663 ± 0.0008
M_* ($M_\odot$)	1.35 ± 0.05
R_* ($R_\odot$)	1.6 ± 0.1
$\log g_*$ (cgs)	4.17 ± 0.04
ρ_* ($\rho_\odot$)	0.34 ± 0.05
$T_{\rm eff}$ (K)	6400 ± 100
[Fe/H]	-0.02 ± 0.05
K (km s^{-1})	0.099 ± 0.009
$M_{\rm P}$ ($M_{\rm Jup}$)	1.0 ± 0.1
$R_{\rm P}$ ($R_{\rm Jup}$)	1.15 ± 0.09
$\log g_{\rm P}$ (cgs)	3.2 ± 0.1
$T_{\rm eql}$ (K)	1500 ± 50

Parameters from RM and DT Analyses:

Parameter (Unit)	DT Value (adopted):	RM Value:
γ (km s^{-1})	0.82 ± 0.01	0.823 ± 0.009
λ (°)	21 ± 6	23 ± 12
$v_{\rm FWHM}$ (km s^{-1})	10 ± 1	…
$v \sin i_*$ (km s^{-1})	13.3 ± 0.6	14.1 ± 0.7

4. Combined Markov Chain Monte Carlo Analysis

We conduct an analysis very similar to that conducted by Temple et al. (2018) for WASP-174b, which involves the use of Markov chain Monte Carlo (MCMC) methods to analyze the combined photometric and spectroscopic data sets. As one approach we use the in-transit spectroscopy data in the form of RV measurements, following the method of Hirano et al. (2011), and as a second approach we use the same data in the form of CCFs, following methods similar to that used by Brown et al. (2017) and Temple et al. (2017). We call the former the RM analysis and the latter the tomographic analysis.
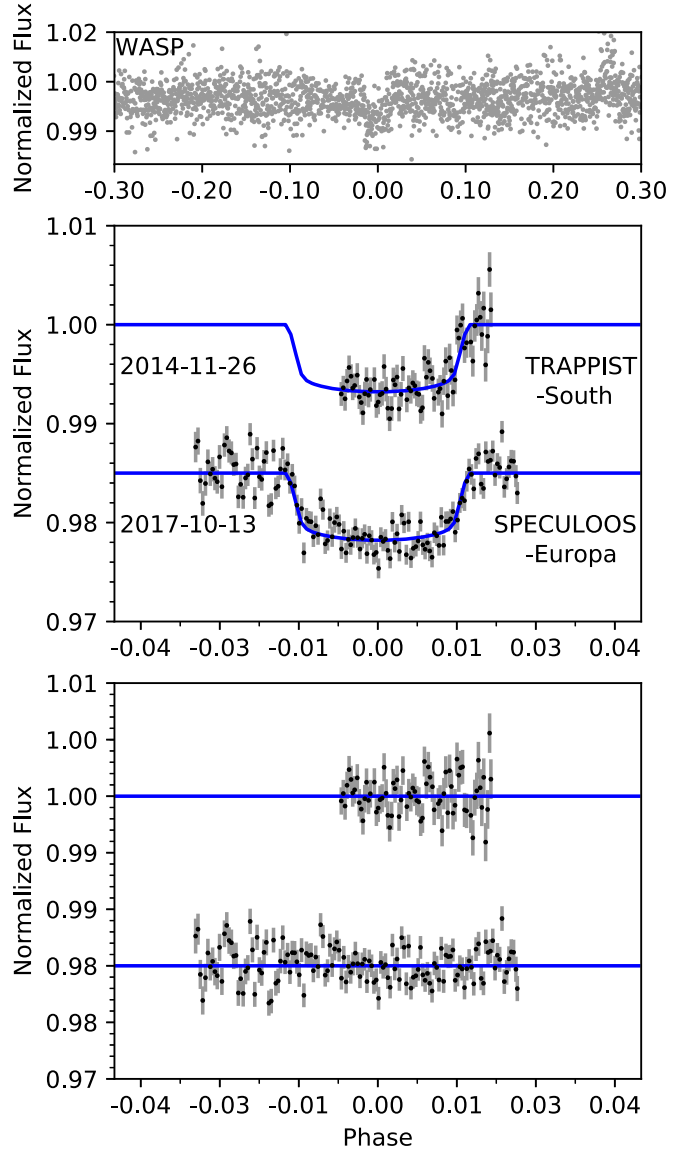

Figure 1. Top: the discovery light curve for WASP-190b (WASP-South). Middle: the two follow-up light curves with the best-fitting model shown in blue. Bottom: the residuals of the fits to the follow-up light curves. The data used to create this figure are available.

The code we use is described by Collier Cameron et al. (2007) and Pollacco et al. (2008), which in the latest version includes the tomographic analysis as described by Collier Cameron et al. (2010a). In both analyses, fitting the photometric light curves allows direct measurement of the planet-to-star area ratio, $(R_{\rm p}/R_\star)^2$, the impact parameter b, and the key transit timing information $T_{\rm c}$, P, T_{14}, and by extension T_{12}, which are respectively the epoch of mid-transit, the orbital period, the transit duration, and the duration of ingress (or equivalently egress). We use the value of $T_{\rm eff}$ obtained in the spectral analysis (see the discussion in Section 7) as the starting value for the MCMC chains, and for each new value of $T_{\rm eff}$ we interpolate four-parameter law limb-darkening coefficients from the tables of Claret (2000, 2004). Stellar mass is calculated at each step using the Enoch–Torres relation (Enoch & Collier Cameron 2010; Torres et al. 2010). The photometric
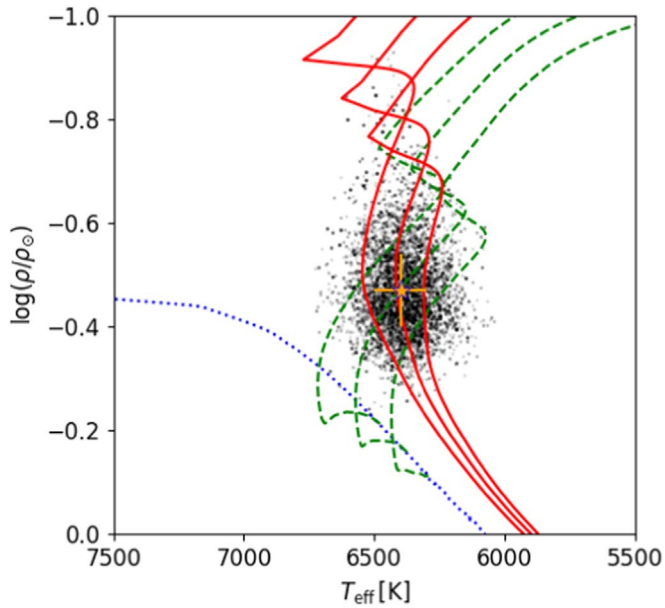
Figure 2. The best-fitting evolutionary tracks and isochrones of WASP-190 obtained using BAGEMASS. Black points: individual realizations of the MCMC. Dotted blue line: Zero-age main sequence (ZAMS) at best-fit [Fe/H]. Green dashed lines: evolutionary track for the best-fit [Fe/H] and mass, plus 1σ bounds. Red lines: isochrone for the best-fit [Fe/H] and age, plus 1σ bounds. Orange star: measured values of $T_{\rm eff}$ and ρ_* for WASP-190 obtained in the spectral and photometric analyses, respectively.

Table 4
Parameters for WASP-190 from BAGEMASS

Parameter (Unit)	Value
Age (Gyr)	2.8 ± 0.4
M_* ($M_\odot$)	1.30 ± 0.05
[Fe/H]$_{\rm init}$	0.03 ± 0.04

data are displayed in Figure 1 along with the best-fit model and residuals of the fit.

The RV analysis then enables measurement of the barycentric system velocity γ and the stellar reflex velocity semi-amplitude K. We expect that most hot Jupiters will settle into a circular orbit on a shorter timescale than their lifetimes (Pont et al. 2011), but with an orbital period of ~ 5 days, WASP-190b is entering the regime where eccentricity may remain. However, we do not have sufficient orbital RVs to constrain the eccentricity and so assume a circular orbit. We do not include the CORALIE measurements in the model adopted here, although including them changes the planetary mass by much less than the error bar.

Both the RM analysis and the tomographic analysis can allow the measurement of $v \sin i_*$ and λ, while providing an additional constraint on the values of γ and b. However, it can often be the case that for the RM analysis a prior on $v \sin i_*$ is required in order to obtain a well-constrained fit, and so we adopt the spectral $v \sin i_*$ as a prior for both analyses. In the tomographic analysis we also fit the local line width, $v_{\rm FWHM}$, resulting from stellar turbulence and instrumental broadening, which influences the width of the planetary perturbation of the line profiles, and whose shape is assumed to be Gaussian.

We show all RV measurements used in this work, along with the best-fitting RV and RM models in Figure 3. We also display the tomographic data (the time series of CCFs with the
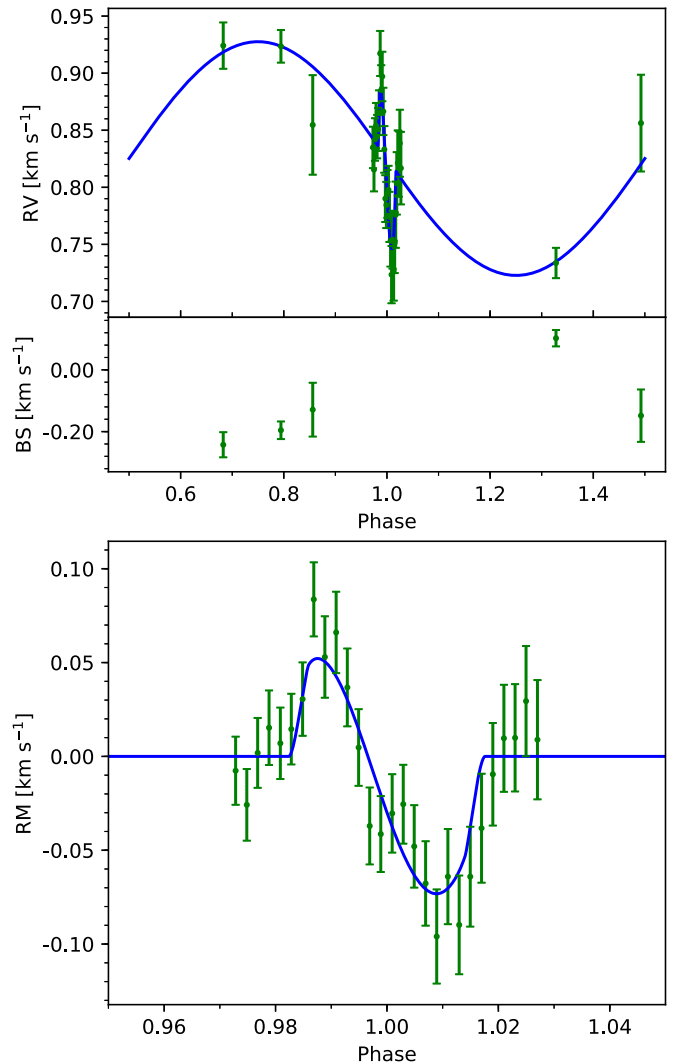

Figure 3. Top: HARPS RV measurements used in the analysis of WASP-190b. The blue line shows the best-fit Keplerian RV curve and the fit to the RM effect. Center: the bisectors for the out-of-transit RVs plotted against phase, which show no correlation with the RV measurements. Bottom: region around transit on a larger scale.

average of the out-of-transit CCFs subtracted from all CCFs) in Figure 4, along with the best-fit planet model and residuals. The best-fit parameters are listed in Table 3. We adopt the solution to the tomographic analysis (see Section 6) and, to avoid duplicating parameters derived from the same data (which are consistent in any case), the only parameters for which we list values from both analyses are γ, $v \sin i_*$, and λ.

5. Results for the Star

We find WASP-190 to have a large radius of $R_* = 1.6 \pm 0.1\, R_\odot$ and a density of $\rho_* = 0.34 \pm 0.05\, \rho_\odot$. This implies that the star is beginning to evolve away from the main sequence, which would be consistent with the spectral type of F6 IV–V.

The effective temperature ($T_{\rm eff}$) was also obtained using the infrared flux method (IRFM; Blackwell & Shallis 1977). The stellar spectral energy distribution was obtained using literature broadband photometry from 2MASS (Skrutskie et al. 2006), APASS9 B, V, g', r', and i' (Henden et al. 2015), USNO-B1 R (Monet et al. 2003), and *WISE* (Cutri et al. 2012). The photometry was converted to fluxes and the best-fitting Kurucz (1993) model
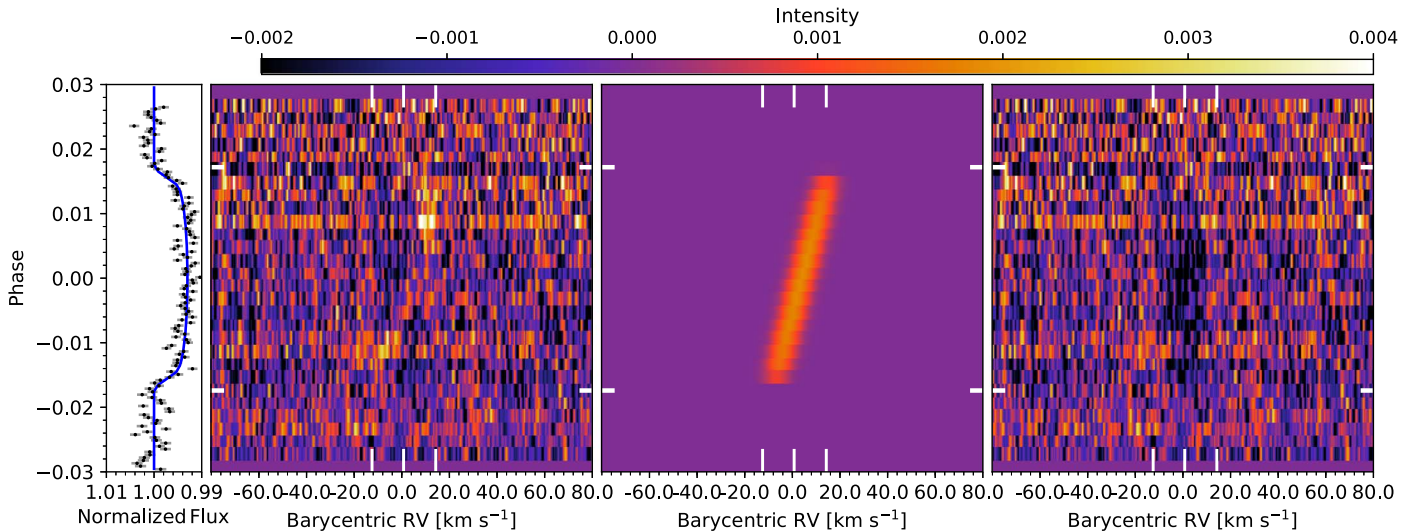
Figure 4. Center-left: Doppler tomogram comprised of the time series of residual HARPS CCFs calculated by subtracting the average of the out-of-transit CCFs from all CCFs. Left: SPECULOOS-Europa light curve taken simultaneously with the HARPS observation. Center-right: best-fit planet model. Right: residuals remaining after subtracting the best-fit planet model from the center-left tomogram. In the three tomographic panels, the start and end times of the transit are marked with horizontal white dashes, while the vertical dashes mark, respectively, the positions of $\gamma - v \sin i_\star$, γ, and $\gamma + v \sin i_\star$. We interpret the tomogram as showing a very faint, prograde planet signal, which in places is completely masked by background noise.
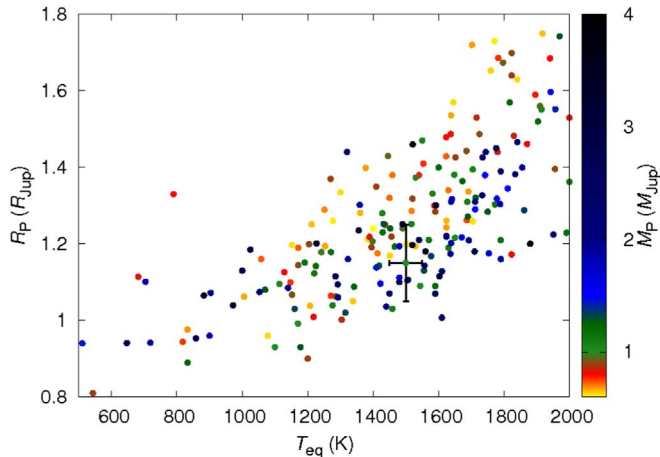
Figure 5. R_p vs. T_{eql}, color coded by mass, of all known planets with $0.6\,M_{Jup} < M_p < 4.0\,M_{Jup}$. WASP-190b is displayed including the error bars on the measured radius and temperature.

flux distribution found and integrated to determine a bolometric flux of $5.27 \pm 0.26 \times 10^{-10}\,erg\,s^{-1}\,cm^{-2}$. No visible interstellar lines were seen around the Na D line, so $E(B-V)$ was assumed to be zero. The IRFM was then used, with the 2MASS fluxes, to obtain a value of $T_{eff} = 6560 \pm 140\,K$ as well as an angular diameter of $\theta = 0.029 \pm 0.001$ mas. The *Gaia* DR2 (Gaia Collaboration et al. 2016, 2018) lists the parallax of WASP-190 as 1.82 ± 0.03 mas. Using these values and accounting for the correction to *Gaia* DR2 parallax values suggested by Stassun & Torres (2018), we obtain a stellar radius of $1.65 \pm 0.08\,R_\odot$, which is consistent with our result from the MCMC analysis.

We investigate the age of WASP-190 using the open source software BAGEMASS[12] (Maxted et al. 2015). BAGEMASS allows the user to fit T_{eff} and $M_\star$ using stellar evolutionary models calculated for different He abundances and mixing lengths (GARSTEC; Weiss & Schlattl 2008). As inputs we use the

values of T_{eff} and [Fe/H] derived from the spectral analysis in Section 3, and also use the value of $\rho_\star$ obtained in the combined analysis (Section 4) as a constraint.

Assuming solar values for the He abundance and mixing length gave the best-fit solution. We display the corresponding isochrones and evolutionary tracks in Figure 2, and give the fitted parameters in Table 4. We find the current age of WASP-190 to be 2.8 ± 0.4 Gyr, implying that the star is beginning to evolve off the main sequence. This is consistent with our finding that the star has a radius larger than expected for a main-sequence star. For comparison, the time taken to exhaust all hydrogen in the core is 3.8 ± 0.5 Gyr.

6. Results for the Planet

We find a best-fit K of $0.099 \pm 0.009\,km\,s^{-1}$, giving a planet mass of $M_p = 1.0 \pm 0.1\,M_{Jup}$. The fitted planetary radius is $1.15 \pm 0.09\,R_{Jup}$.

The in-transit RVs, showing the RM effect, are displayed in the lower panel of Figure 3. The equivalent tomogram of the same data is shown in Figure 4. Both are consistent with a planet in a prograde orbit. The projected spin–orbit angle, λ, is measured as $23° \pm 12°$ in the RM analysis and as $21° \pm 6°$ in the tomographic analysis. The planet trace is faint and hard to see, which we attribute to the star being relatively faint for tomographic analysis, at $V = 11.7$, and the transit dip being relatively shallow for a hot Jupiter, at 0.6%. The latter results from the star being relatively large at $1.6\,R_\odot$ when compared to the planet, which has only a mildly inflated radius of $1.15\,R_{Jup}$.

7. Discussion and Conclusions

We have shown that WASP-190b is a typical hot Jupiter with a mass of $1.0 \pm 0.1\,M_{Jup}$ and a mildly inflated radius of $1.15 \pm 0.09\,R_{Jup}$. It is in a 5.4-day orbit that is marginally misaligned with respect to the stellar rotation, with $\lambda = 21° \pm 6°$.

The measured values of $v \sin i_\star$ and λ are consistent between the spectral analysis, the tomographic analysis, and the RM

analysis. The tomographic analysis produced similar fits, giving a $v \sin i_\star$ value consistent with the spectroscopic value, regardless of whether we adopted the spectroscopic $v \sin i_\star$ as a prior. In contrast, the RM analysis was less constrained without a prior, and the fit tended to favor values that were too large. This often occurs for systems with a low impact parameter b, since it is difficult to differentiate the effects of $v \sin i_\star$ and λ on the shape of the RM curve when it is symmetrical (e.g., Albrecht et al. 2011). Since, in WASP-190, the impact parameter has a mid-level value of $b = 0.45$, this tendency should be reduced, but it may be that the low signal-to-noise of the data is leading the fit to be less constrained than usual. Overall, we found that the parameters were better constrained in the tomographic analysis than in the RM analysis, and so we adopt that fit.

While there is a well-established trend between the irradiation of a hot Jupiter and the inflation of its radius (e.g., Enoch et al. 2012), hot Jupiters also display a wide range of radii (e.g., Burrows et al. 2007). Sestovic et al. (2018) investigates the relationship between planet radius, mass, and irradiation, finding that a more massive planet is usually less inflated than a low-mass planet of the same temperature, due to the planet's gravity counteracting the inflation. In Figure 5 we show planetary radius as a function of equilibrium temperature, and use planetary mass as a third dimension, for all planets with $0.6\,M_{\mathrm{Jup}} < M_{\mathrm{p}} < 4.0\,M_{\mathrm{Jup}}$ as listed in the TEPCat database (Southworth 2011). The figure indicates that planets of a given mass and equilibrium temperature can have a wide range of radii, and shows that planets of $\sim 1\,M_{\mathrm{Jup}}$ like WASP-190b are not necessarily inflated, implying that the invocation of some third parameter is required. Possible causes of the disparity include different evolutionary histories, leading to different amounts of irradiation over time (e.g., Hartman et al. 2016), the possibility of internal heating mechanisms (e.g., Ginzburg & Sari 2015; Kurokawa & Inutsuka 2015; Ryu et al. 2018; Thorngren & Fortney 2018), and differences in the mass and metallicity of the planets' cores (e.g., Enoch et al. 2012).

With $\lambda = 21° \pm 6°$, WASP-190b is marginally misaligned. This is consistent with the known trend in hot-star systems, whereby planets around stars beyond the Kraft break have a wider range of obliquities, with most being in misaligned orbits (e.g., Winn et al. 2010; Dai & Winn 2017). The true orbit may be more strongly misaligned, however, since the value of $|\lambda|$ for non-polar misaligned orbits represents a lower limit for the true obliquity $|\psi|$. To measure ψ it would be necessary to independently measure the stellar equatorial rotational velocity v or stellar inclination $i_\star$ (for example, by looking for differential rotation effects as described by Cegla et al. 2016).

ORCID iDs

C. Hellier ⓘ https://orcid.org/0000-0002-3439-1439
D. R. Anderson ⓘ https://orcid.org/0000-0001-7416-7522
D. J. A. Brown ⓘ https://orcid.org/0000-0003-1098-2442
M. Gillon ⓘ https://orcid.org/0000-0003-1462-7739
M. Lendl ⓘ https://orcid.org/0000-0001-9699-1459
P. F. L. Maxted ⓘ https://orcid.org/0000-0003-3794-1317
D. Pollacco ⓘ https://orcid.org/0000-0001-9850-9697
D. Queloz ⓘ https://orcid.org/0000-0002-3012-0316
D. Ségransan ⓘ https://orcid.org/0000-0003-2355-8034
B. Smalley ⓘ https://orcid.org/0000-0002-3456-087X
A. H. M. J. Triaud ⓘ https://orcid.org/0000-0002-5510-8751

References

Albrecht, S., Winn, J. N., Johnson, J. A., et al. 2011, ApJ, 738, 50
Anderson, D. R., Temple, L. Y., Nielsen, L. D., et al. 2018, arXiv:1809.04897
Baranne, A., Queloz, D., Mayor, M., et al. 1996, A&AS, 119, 373
Blackwell, D. E., & Shallis, M. J. 1977, MNRAS, 180, 177
Boué, G., Montalto, M., Boisse, I., Oshagh, M., & Santos, N. C. 2013, A&A, 550, A53
Brown, D. J. A., Triaud, A. H. M. J., Doyle, A. P., et al. 2017, MNRAS, 464, 810
Bruntt, H., Bedding, T. R., Quirion, P.-O., et al. 2010, MNRAS, 405, 1907
Burdanov, A., Delrez, L., Gillon, M., & Jehin, E. 2018, in Handbook of Exoplanets, ed. H. J. Deeg & J. A. Belmonte (Cham: Springer), 130
Burrows, A., Hubeny, I., Budaj, J., & Hubbard, W. B. 2007, ApJ, 661, 502
Cegla, H. M., Lovis, C., Bourrier, V., et al. 2016, A&A, 588, A127
Claret, A. 2000, A&A, 363, 1081
Claret, A. 2004, A&A, 428, 1001
Collier Cameron, A., Bruce, V. A., Miller, G. R. M., Triaud, A. H. M. J., & Queloz, D. 2010a, MNRAS, 403, 151
Collier Cameron, A., Guenther, E., Smalley, B., et al. 2010b, MNRAS, 407, 507
Collier Cameron, A., Wilson, D. M., West, R. G., et al. 2007, MNRAS, 380, 1230
Crouzet, N., McCullough, P. R., Long, D., et al. 2017, AJ, 153, 94
Cutri, R. M., et al. 2012, yCat, 2311
Dai, F., & Winn, J. N. 2017, AJ, 153, 205
Delrez, L., Gillon, M., Queloz, D., et al. 2018, Proc. SPIE, 10700, 107001I 21
Doyle, A. P., Davies, G. R., Smalley, B., Chaplin, W. J., & Elsworth, Y. 2014, MNRAS, 444, 3592
Enoch, B., Collier Cameron, A., & Horne, K. 2012, A&A, 540, A99
Enoch, B., Collier Cameron, A., Parley, N. R., & Hebb, L. 2010, A&A, 516, A33
Gaia Collaboration, Brown, A. G. A., Vallenari, A., et al. 2018, A&A, 616, A1
Gaia Collaboration, Prusti, T., de Bruijne, J. H. J., et al. 2016, A&A, 595, A1
Gillon, M. 2018, NatAs, 2, 344
Ginzburg, S., & Sari, R. 2015, ApJ, 803, 111

Gray, R. O., & Corbally, C. J. 2014, AJ, 147, 80
Hartman, J. D., Bakos, G. Á, Bhatti, W., et al. 2016, AJ, 152, 182
Hellier, C., Anderson, D. R., Collier Cameron, A., et al. 2011, EPJWC, 11, 01004
Henden, A. A., Levine, S., Terrell, D., & Welch, D. L. 2015, AAS Meeting, 225, 336.16
Hirano, T., Suto, Y., Winn, J. N., et al. 2011, ApJ, 742, 69
Jehin, E., Gillon, M., Queloz, D., et al. 2011, Msngr, 145, 2
Kurokawa, H., & Inutsuka, S.-i. 2015, ApJ, 815, 78
Kurucz, R. 1993, SYNTHE Spectrum Synthesis Programs and Line Data (Cambridge, MA: SAO), 13
Lund, M. B., Rodriguez, J. E., Zhou, G., et al. 2017, AJ, 154, 194
Maxted, P. F. L., Anderson, D. R., Collier Cameron, A., et al. 2011, PASP, 123, 547
Maxted, P. F. L., Serenelli, A. M., & Southworth, J. 2015, A&A, 575, A36
Monet, D. G., Levine, S. E., Canzian, B., et al. 2003, AJ, 125, 984
Pepe, F., Mayor, M., Rupprecht, G., et al. 2002, Msngr, 110, 9
Pollacco, D., Skillen, I., Collier Cameron, A., et al. 2008, MNRAS, 385, 1576
Pont, F., Husnoo, N., Mazeh, T., & Fabrycky, D. 2011, MNRAS, 414, 1278
Queloz, D., Eggenberger, A., Mayor, M., et al. 2000, A&A, 359, L13
Queloz, D., Mayor, M., Udry, S., et al. 2001, Msngr, 105, 1

Ricker, G. R., Winn, J. N., Vanderspek, R., et al. 2015, JATIS, 1, 014003
Ryu, T., Zingale, M., & Perna, R. 2018, MNRAS, 481, 5517
Schlaufman, K. C. 2018, ApJ, 853, 37
Sestovic, M., Demory, B.-O., & Queloz, D. 2018, A&A, 616, A76
Skrutskie, M. F., Cutri, R. M., Stiening, R., et al. 2006, AJ, 131, 1163
Southworth, J. 2011, MNRAS, 417, 2166
Stassun, K. G., Oelkers, R. J., Pepper, J., et al. 2018, AJ, 156, 102
Stassun, K. G., & Torres, G. 2018, ApJ, 862, 61
Talens, G. J. J., Albrecht, S., Spronck, J. F. P., et al. 2017, A&A, 606, A73
Temple, L. Y., Hellier, C., Albrow, M. D., et al. 2017, MNRAS, 471, 2743
Temple, L. Y., Hellier, C., Almleaky, Y., et al. 2018, MNRAS, 480, 5307
Thorngren, D. P., & Fortney, J. J. 2018, AJ, 155, 214
Torres, G., Andersen, J., & Giménez, A. 2010, A&ARv, 18, 67
Triaud, A. H. M. J. 2017, in Handbook of Exoplanets, ed. H. J. Deeg & J. A. Belmonte (Cham: Springer), 1
Weiss, A., & Schlattl, H. 2008, Ap&SS, 316, 99
Winn, J. N., Fabrycky, D., Albrecht, S., & Johnson, J. A. 2010, ApJL, 718, L145
Yadav, R. K., & Thorngren, D. P. 2017, ApJL, 849, L12
Zhou, G., Bakos, G. Á, Hartman, J. D., et al. 2017, AJ, 153, 211